Acta Materialia 124 (2017) 71–78

Contents lists available at ScienceDirect

Acta Materialia

journal homepage: www.elsevier.com/locate/actamat

Full length article

Ion-irradiation induced clustering in W-Re-Ta, W-Re and W-Ta alloys: An atom probe tomography and nanoindentation study

Alan Xu [a, b], David E.J. Armstrong [a, *], Christian Beck [a], Michael P. Moody [a], George D.W. Smith [a], Paul A.J. Bagot [a], Steve G. Roberts [a, c]

[a] University of Oxford, Department of Materials, Parks Road, Oxford, OX1 3PH, UK
[b] Nuclear Fuel Cycle, Australian Nuclear Science and Technology Organisation, New Illawarra Road, Lucas Heights, NSW, 2234, Australia
[c] Culham Centre for Fusion Energy, Culham Science Centre, Abingdon, OX14 3DB, UK

ARTICLE INFO

Article history:
Received 1 June 2016
Received in revised form
24 September 2016
Accepted 20 October 2016
Available online 4 November 2016

Keywords:
Tungsten rhenium tantalum alloys
Nuclear fusion
Atom probe tomography
Ion-irradiation
Nanoindentation

ABSTRACT

In tungsten plasma-facing fusion reactor components, Ta is the third most abundant element formed by transmutation (after Re and Os), yet little is known about the behaviour of W-Ta alloys under irradiation and any effects Ta might have on Re clustering in W-Re-Ta alloys. In this study, W−4.5 at.%Ta, W−2 at.% Re−1 at.%Ta and W−2 at.%Re alloys were exposed to 2 MeV W+ ions to a fluence of 2.64×10^{15} ions cm^{-2} at temperatures of 573 and 773 K. Atom probe tomography and nanoindentation were used to characterise the chemical and physical properties of the irradiation-induced clusters and the mechanical properties of the irradiated layer. In the W-Ta alloy, no evidence of irradiation-induced clustering was found. In the W−Re−Ta alloy, at both irradiation temperatures studied the presence of Ta reduced the W-Re cluster number density and volume fraction compared to that in the W-Re alloy; however it did not alter cluster composition as the Ta was rejected from the clusters. The reduced cluster density in the W-Re-Ta alloys was associated with a smaller degree of irradiation hardening than in the W-Re alloys. Possible mechanisms by which Ta hinders cluster development are discussed.

1. Introduction

Tungsten is the leading candidate plasma facing material for any future nuclear fusion reactors, in which it will have to withstand extreme conditions including up to ~1300 K operating temperature, 1–20 MW m^{-2} heat flux and 14 MeV neutron and up to 3.5 MeV He^+ ion bombardment [1–4]. The incident neutrons will cause transmutation of tungsten, predominantly to Re, Os and Ta (in descending order of transmutation rate [5,6]). Exact transmutation rates will depend on the neutron spectrum at any given location in a reactor but neutronics modelling by Gilbert and Sublet using a theoretical fusion neutron spectrum suggest 3 at% Re, 1.4 at% Os and 0.9 at% Ta could be produced in tungsten after 5 years in a typical first wall position. Neutron irradiation can also lead to radiation-induced precipitation at solute concentrations where a solid solution would be expected at thermal equilibrium [7–11], giving rise to solute clustering and formation of ordered σ and χ phases [7,12]. The presence of these clusters and precipitates can significantly harden the tungsten, may induce embrittlement and may severely reduce component lifetime [7,8,13,14].

These neutron irradiation-enhanced transmutation element clustering and hardening effects can be physically modelled by study of ion-irradiated W alloys containing suitable concentrations of the transmutation elements. Clustering and hardening is found to occur in ion-irradiated binary W-Re alloys [15], and is further enhanced by the presence of osmium [16]. In a W−1Re−1Os alloy, ion-irradiated to 33 dpa at 773 K, the solute cluster density was higher by a factor of 3, and the irradiation-induced hardening was 1.54 GPa higher, than in an identically irradiated W-2Re alloy [16,17]. This shows that synergistic effects between various solute species within tungsten alloys are of major importance during the formation and growth of clusters and precipitates. This is the reason for this comparative study of W-Re, W-Ta and W-Re-Ta alloys.

Mechanical tests have shown that alloying W with Ta has an embrittling effect even in the absence of radiation. Rieth et al. performed Charpy impact tests on pure W and W−5 at.%Ta alloy specimens [2]. The brittle-ductile transition temperature (BDTT) of

* Corresponding author.
E-mail address: david.armstrong@materials.ox.ac.uk (D.E.J. Armstrong).

http://dx.doi.org/10.1016/j.actamat.2016.10.050

the pure W was 623–723 K, and that of the W-Ta alloy was 1173–1273 K. Below the BDTT, the W–Ta alloy failed in a brittle intergranular manner. Armstrong et al. performed nanoindentation measurements on pure W and a W–5Ta alloy, W-ion irradiated to doses ranging from 0 to 33 dpa at 573 K [18,19]. In pure W, the irradiation induced hardening saturated above a damage level of 0.4 dpa and with a radiation-induced increase in hardness (≈0.8 GPa) lower than in the W-Ta alloy, which did not saturate until damage levels above 13dpa and showed a hardness increase of ≈3.8 GPa. However, no post-irradiation microstructural examination of these W-5Ta alloys was performed, so the mechanism for this large increase in hardness could not be determined.

The work reported here investigates the effects of Ta on Re clustering and precipitation in W-based alloys during ion irradiation, using Atom Probe Tomography (APT) to examine the microstructures and nanoindentation to study the associated hardness changes.

2. Experimental

Three alloy compositions were investigated: W–2Re–1Ta, W–2Re and W–4.5Ta (all nominal compositions in atomic %). The ternary composition was chosen to approximate the level of Re and Ta transmutation products after 5 years of DEMO fusion reactor operation [5,6] (osmium would also be produced, but its effects do not form part of this study). The binary W-Re alloy has the same Re content as the ternary, so as to compare clustering behaviour in the presence and absence of Ta. The W-Ta binary alloy was used to study the clustering characteristics of Ta in W alone.

The three alloys were all manufactured at Oxford University, UK. Powders of high purity (99.9 at.%) W, Re and Ta (Sigma Aldrich Ltd) were blended, vacuum arc melted and solidified into hemispheroidal ingots of 10–20 mm diameter. The ingots were cut into 1 mm thick slices using a diamond saw and then ground and polished, the final polish being with 45 nm colloidal silica particles. All alloys featured large equiaxed grains of 0.5–2 mm diameter. Table 1 shows overall Atom Probe Tomography (APT) and Electron Probe Microanalysis (EPMA) compositional analyses of the alloys.

Two self-ion (W+) irradiation experiments were undertaken at the National Ion Beam Centre, University of Surrey, UK, exposing the samples to a 2 MeV W^+ beam to a fluence of 2.64×10^{15} ions cm^{-2} at a flux of 1.96×10^{10} ions $cm^{-2}s^{-1}$, at 573 and 773 K. These temperatures were chosen to lie above and below the critical temperature for stage III (vacancy-controlled) recovery of 743 K in pure tungsten [20]. SRIM simulations [21] using a displacement energy of 68 eV [18,19,22] predict a maximum damage level of 33 dpa, with the damage profile extending to 300 nm below the surface.

Atom probe needles were fabricated from irradiated and non-irradiated alloys via the lift–out process using a Zeiss Nvision 40 Focused Ion Beam system. The sample surface was coated with a protective layer of carbon and cantilevers 2 × 10 μm and 4 μm deep were milled perpendicular to the surface. The cantilevers were lifted out of the sample surface, mounted onto flat-top 2 μm diameter Si posts and annular milled to 50–100 nm apex diameter. A detailed description is given by Thompson et al. [23,24]. A minimum of 3 needles was studied for each irradiation condition. A LEAP 3000X HR atom probe was used to analyse the materials, operating in laser mode with pulse energy of 0.6–0.8 nJ and stage temperature of 50 K. Data were reconstructed using IVAS 3.6.6 software. A high density <110> pole was present in all the reconstructions and was used to calibrate depth analyses by fitting the {110} lattice plane spacing to the known value for W of 0.22 nm [3,25].

Solute clusters were identified using a maximum separation algorithm [26,27]. In this approach any pairs of solute atoms separated by a distance less than the user-specified “d-max” value are identified as part of the same cluster. After this step, any of the resulting solute clusters containing fewer atoms than a defined “Nmin” value are discarded. For all cluster analyses presented in this study, dmax and Nmin values were determined for each dataset analysed using the calibration procedure detailed in Ref. [16]; the d-max value ranged between 1.00 nm and 1.50 nm and Nmin was 20 in all cases.

The hardness of the alloys was measured with a Nanoindenter XP using a diamond Berkovich tip, calibrated against fused silica. The Continuous Stiffness Method (CSM) [28] was used to measure the hardness as a function of depth up to a depth of 1 μm, in order to cover the 300 nm damage region predicted by SRIM. The hardness data were averaged across a minimum of 16 indents taken over at least 3 grains. Hardness values reported are from an indentation depth of 125 nm, allowing comparison to be made between samples without effects from the softer unimplanted material beneath [19,28].

Table 1
Composition for W-2Re-1Ta, W-2Re and W-4.5Ta alloys as measured using Atom Probe and EPMA. W is the balance.

Alloy	Analysis type	Re (at.%)	Ta (at.%)
W-2Re-1Ta	Atom Probe	2.0	0.8
W-2Re	Atom Probe	2.1	–
W-2Re	EPMA	1.9	–
W-4.5Ta	Atom Probe	–	4.4
W-4.5Ta	EPMA	–	4.5

3. Results

3.1. Atom probe analysis

3.1.1. Comparison with SRIM predictions

Fig. 1a) shows 3D reconstructions of the analysed volume of a W-2Re-1Ta alloy irradiated to 33dpa at 773 K. To improve the image quality, only 2% of total W atoms are shown while 50% of the total solute Re and Ta atoms are displayed. The top atom map shows W only while the middle and bottom atom maps show the Re and Ta

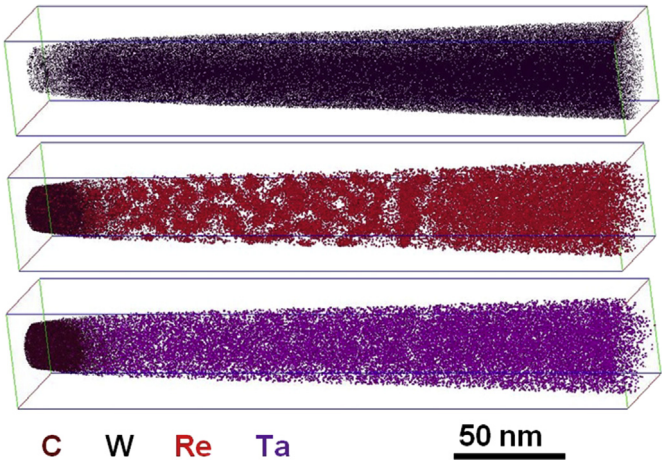

Fig. 1. a) Full 3D atom reconstructions of W-2Re-1Ta irradiated to 33dpa at 773 K, showing one element per atom map: Tungsten (top), Re (middle) and Ta (bottom) along with brown carbon cap. b) Plots of ion damage (SRIM) as well as cluster volume and diameter against reconstruction depth. (For interpretation of the references to colour in this figure legend, the reader is referred to the web version of this article.)

atoms individually. The carbon cap (brown atoms) is present in Re and Ta atom maps and marks the original material surface. The carbon cap is omitted in the W atom map, showing that the interface between the carbon cap and substrate is not sharp; there is a ~25 nm region where both C and W are present as a result of knock-in effects during C deposition. Of the three elements, only Re exhibits clustering. Fig. 1b) shows the corresponding Re average cluster diameters and volume fractions as a function of depth from the original surface, with data points measured at 10 nm intervals. At ~150 nm below the sample surface the measured mean cluster diameter was ~7–8 nm, and the volume fraction ~15%. Clustering reduces below ~150 nm depth, and is not apparent at 300 nm depth. These trends correlate well with the predicted SRIM damage profile also shown in Fig. 1b).

3.1.2. Effect of Ta on Re clustering

Fig. 2a–d) shows the atomic distribution within a 4 nm thick slice of an APT reconstruction of the subsurface damage regions (depth less than 150 nm) in W-2Re-1Ta and W-2Re specimens irradiated to 33 dpa at 573 and 773 K (Re - red and Ta – purple). Data on average cluster composition, cluster radius, volume fraction and number density are reported in Table 2. The presence of Ta hinders Re cluster formation at both irradiation temperatures.

After irradiation at 573 K, the Re clusters are less visible in the ternary alloy (Fig. 2a) compared to the binary alloy (Fig. 2b). The measured cluster volume fraction is a factor of three lower in the W-Re-Ta alloy compared to the W-Re alloy, and the cluster number density in the W-Re-Ta alloy is ~60% of that measured in the W-Re binary alloy. The cluster radii and Re content are however similar in the two alloys.

After irradiation at 773 K, in both alloy types, the cluster volume, radii and Re content are higher and the number density lower than for 573 K irradiation. The clusters in the W-Re-Ta and W-Re alloys irradiated at 773 K have similar radius and Re concentrations but the cluster number density and volume fraction in the irradiated ternary alloy are significantly lower than in the binary alloy.

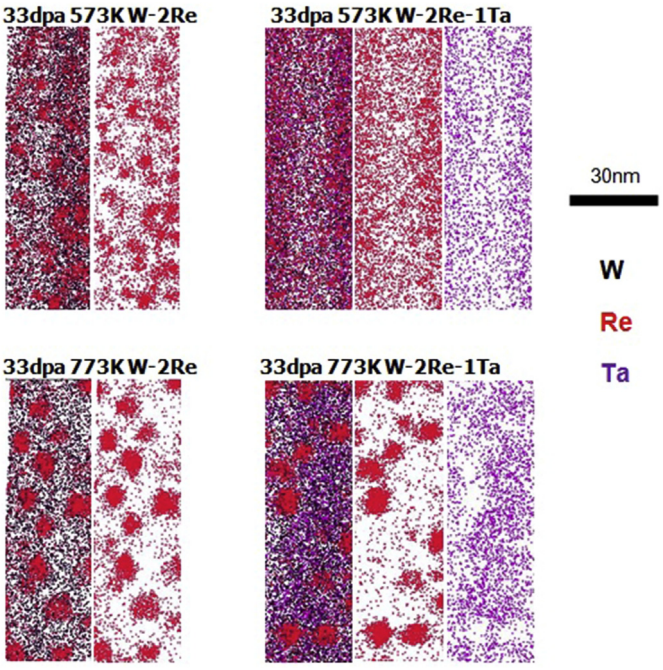

Fig. 2. 4 nm thick sections from atom maps showing distribution of atomic species distribution following W-ion irradiation to 33dpa in a) W–2Re at 573 K, b) W–2Re at 773 K, c) W–2Re–1Ta at 573 K, d) W–2Re–1Ta at 773 K. W, Re and Ta atoms are shown in black, red and purple respectively. The W-2Re atom maps are taken from Ref. [16]. (For interpretation of the references to colour in this figure legend, the reader is referred to the web version of this article.)

3.1.3. Cluster structure

The proxigram analyses in Fig. 3a–b) shows the radial Re concentration, measured at 0.2 nm intervals and averaged for 10 median radius clusters (identified with a 4 at.% Re iso-surface). The Re concentration profiles for W-Re-Ta and W-Re alloys are similar for the two irradiation temperatures. They both feature a smooth decrease in Re concentration with radial distance. The concentrations at the cluster core for 573 K and 773 K irradiation temperatures are 12 and 27 at.% Re respectively, well below the σ phase composition of 50 at.% Re [29,30].

To further investigate the nature of the clusters, a 3 nm thick slice from a cluster formed in the W-2Re-1Ta alloy at 773 K was imaged along the <110> pole of the reconstruction (Fig. 3d). In this atom map, the {110} planes of the tungsten matrix (black atoms) are visible and continuous throughout the cluster and into the matrix. The rhenium and tantalum atoms are displaced from these planes. This is likely due to the known retention of the rhenium atoms on the surface of the needle during evaporation resulting in their correct lattice position to be unclear [31]. The reconstruction is therefore consistent with a model where the clusters are at least semi-coherent, unlike irradiation-induced σ and χ precipitates which are completely incoherent with the BCC matrix [7,29].

The corresponding Ta radial concentration profile for clusters in the W-Re-Ta alloy is shown in Fig. 3c) for both irradiation conditions. At 573 K, the Ta profile shows a slight decrease in solute concentration towards the cluster core. This is further confirmed by Table 2, which shows that 0.77 at.% Ta is the average concentration for clusters in the W-2Re-1Ta alloy. The depletion of Ta within the clusters becomes more significant at 773 K. The Ta concentration drops to zero towards the cluster core; with an overall average Ta concentration of 0.17 at.% (Table 2).

3.1.4. Cluster size distributions

Fig. 4 shows cluster size distribution histograms for W-2Re-1Ta and W-2Re samples irradiated to 33 dpa at 573 and 773 K. The data are based on 500–1000 clusters in each case. To facilitate comparison each plot is normalised to represent the number of clusters in a 1 μm^3 volume. All plots feature a sharp drop in number density below the 0.5–1 nm radius range; this is an artefact of the cluster analysis process, as clusters with solute atoms <20 (Nmin parameter) are discarded.

For the same level of radiation damage, the higher irradiation temperature causes the clusters to coarsen to a greater extent than at the lower temperature. At 773 K, the FWHM of the size distribution for each alloy is approximately double that at 573 K.

3.1.5. Binary W-Ta and W-Re alloys

Fig. 5a) and b) show the distribution of solute atoms within a 4 nm thick slice of the APT reconstruction of the W-4.5Ta and W-2Re alloys, each irradiated to 33 dpa at 573 K. Visually, no significant Ta clustering is apparent in W-4.5Ta, in contrast to the obviously clustered Re atoms in the W-2Re alloy. To quantify this, Fig. 5c) shows the radial concentration distribution averaged across all solute atoms in the atom probe data sets for the W-Ta alloy and the W-2Re alloy irradiated at 573 K. The analysis of the distribution of Ta atoms in the W-Ta produces a flat profile, indicating a homogeneous distribution of this solute species, while in the W-Re alloy, the radial concentration distribution has a maximum at short inter-atomic distances, indicating clustering.

In Fig. 6, the cluster size distributions are plotted for the W-4.5Ta and W-2Re alloys irradiated to 33 dpa at 573 K. Here, a lower Nmin

Table 2
Average cluster characteristics for W-2Re and W-Re-1Ta after irradiation to 33dpa at 573 K and 773 K.

	573 K 33dpa W2Re	773 K 33dpa W2Re	573 K 33dpa W2Re1Ta	773 K 33dpa W2Re1Ta
Re (at.%)	8.0 ± 1.4	12.8 ± 2.9	6.2 ± 1.1	13.6 ± 2.4
Ta (at.%)	–	–	0.77 ± 0.36	0.17 ± 0.12
Radius (nm)	2.4 ± 1.0	3.3 ± 1.9	2.1 ± 0.8	3.4 ± 1.3
Volume fraction (%)	9.01 ± 0.38	11.2 ± 0.7	3.15 ± 0.21	7.11 ± 0.54
Number density (x10^{23} m^{-3})	1.72 ± 0.07	0.81 ± 0.05	1.07 ± 0.07	0.50 ± 0.04

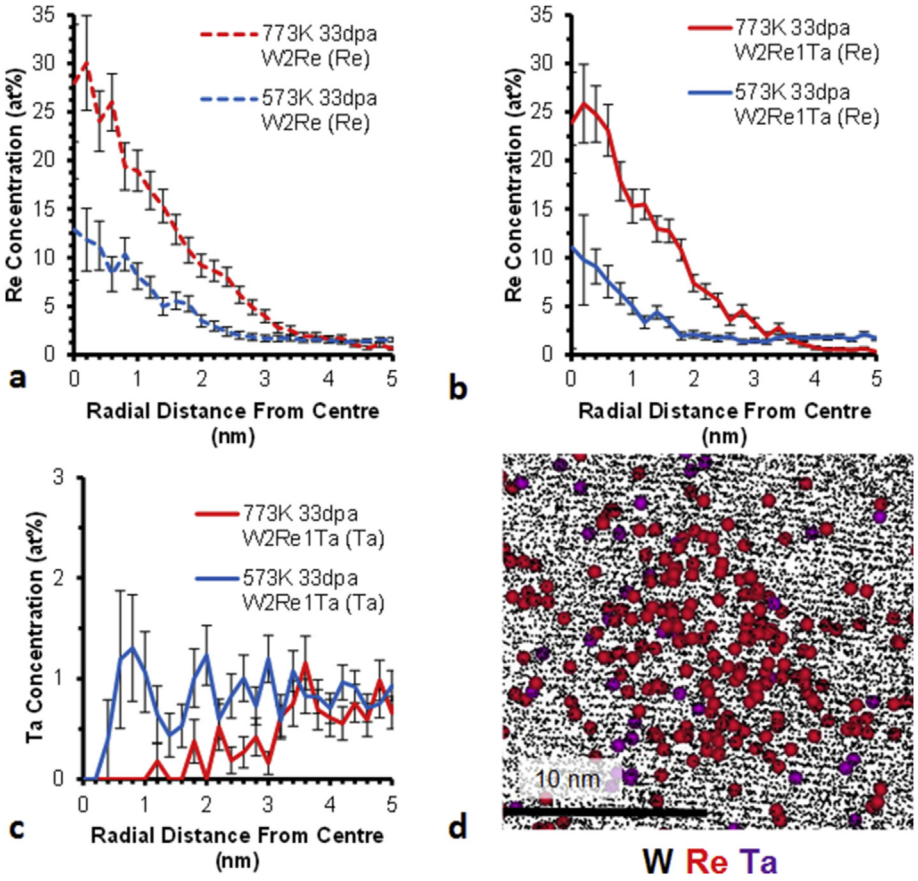

Fig. 3. Proximity histograms at both irradiation conditions showing (a) averaged Re variation within typical clusters in the W–2Re alloy; (b) averaged Re variation within typical clusters in the W–2Re-1Ta alloy; c) averaged Ta variation within typical clusters in the W–2Re-1Ta alloy; (d) a single cluster within W-2Re-1Ta imaged along the <110> direction.

parameter of 5 was used to enable the identification of possible smaller clusters, and the clusters were counted as a function of the number of detected atoms in each, instead of by cluster radius. Each graph shows two plots; an experimental data set and data derived from an artificial, homogeneous data set in which the atom positions of each species were randomised. In the W-4.5Ta alloy, the distribution plots show essentially complete overlap for the randomised and experimental cases, indicating the absence of any significant clustering behaviour. This is unlike the W-2Re alloy, where the distribution plot for the randomised case drops to zero at ~20 atoms while the experimental plot extends beyond 105 atoms, demonstrating strong clustering of Re atoms.

3.2. Irradiation hardening

Fig. 7 and Table 3 show nano-hardness measurements, at 125 nm indenter depth, of the alloy samples pre- and post-irradiation. In the unirradiated state, the presence of Ta has a stronger solid solution hardening effect than that of Re, as reported elsewhere [32,33]. There is negligible hardness difference between the pure W and the W-2Re alloy. The W-4.5 at%Ta alloy and the W-2Re-1Ta alloy are slightly harder than pure W (by ~1 GPa).

The W-4.5Ta alloy irradiated to 33dpa at 573 K experiences an irradiation hardening (relative to unirradiated state) of 2.84 GPa. The irradiation hardening for W-2Re alloy irradiated to 33dpa at 573 K is 3.84 GPa. For the W-4.5Ta alloy, the irradiation hardening/solute content ratio is 0.7 GPa/at.%Ta while for the W-2Re alloy, it is 1.9 GPa/at%.Re. The irradiation hardening may thus be due to a combination of effects from solute clusters (visible directly in the APT data reported here), hardening only the Re-containing materials, and dislocation loops (not directly visible by APT), hardening all materials. This is discussed in section 4.2.

4. Discussion

4.1. Clustering behaviour in W-Re-Ta and W-Ta alloys

The high Ta-content alloy, W-4.5Ta, was studied, to maximise

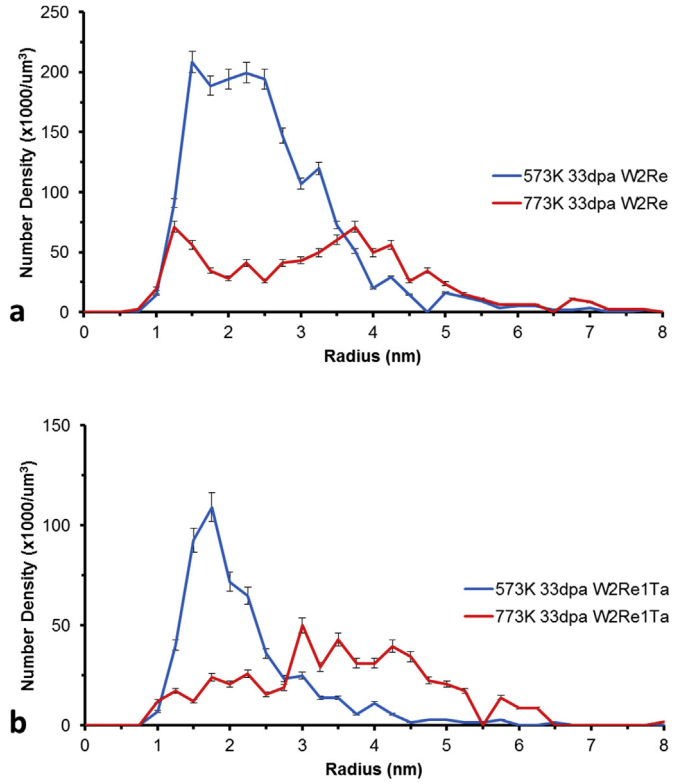

Fig. 4. Normalised cluster radius number density distribution plots for a) W−2Re alloy and b) W−2Re−1Ta at both irradiation conditions.

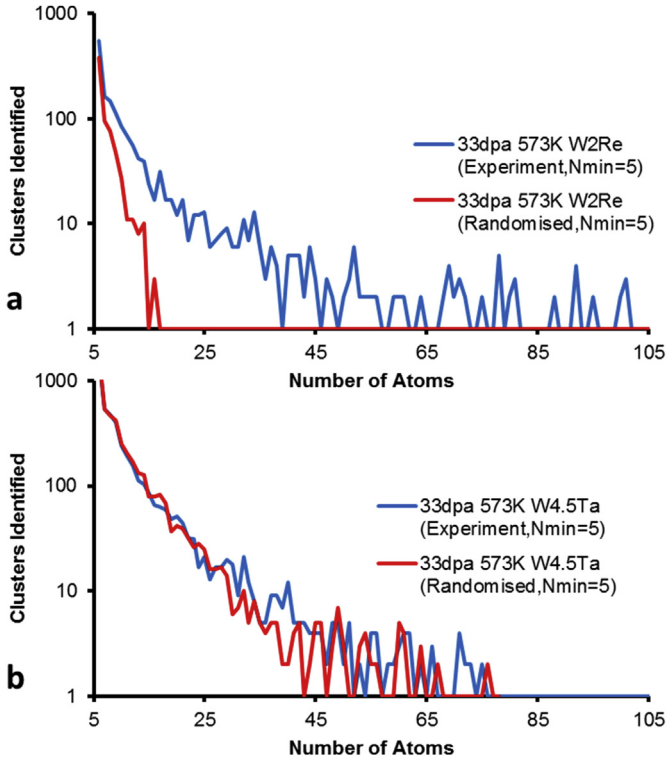

Fig. 6. Cluster size distributions (measured in number of atoms) for (a) Ta in W-4.5Ta and (b) Re in W-2Re alloys, each irradiated to 33 dpa at 573 K. Experimental and mathematically-randomised distributions are shown for comparison purposes.

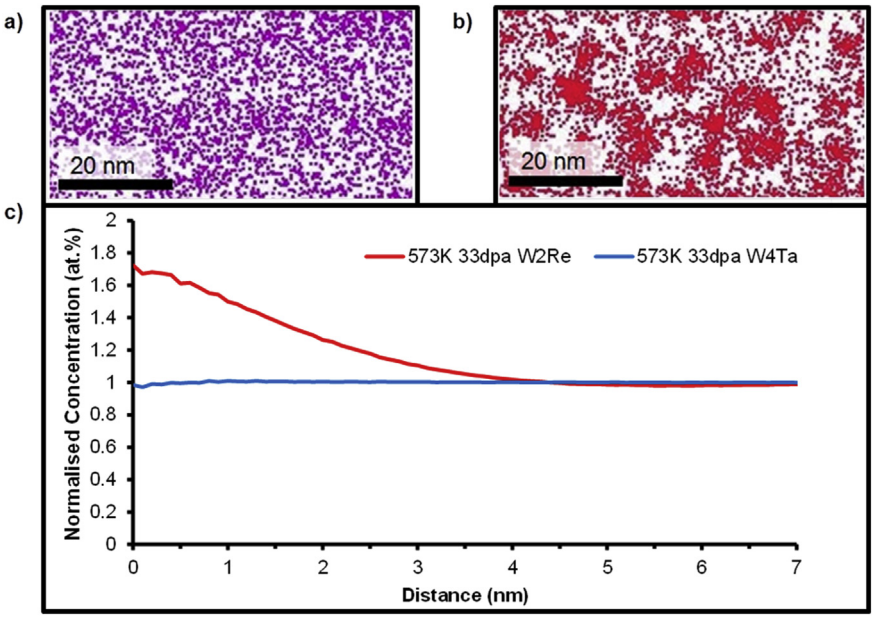

Fig. 5. a) 4 nm thick atom map showing Ta atom distribution for W−4.5Ta irradiated to 33 dpa at 573 K b) 4 nm thick atom map showing Re atom distribution for W−2Ra irradiated to 33 dpa at 573 K c) Radial distribution function plot for Ta atoms in W−4.5Ta irradiated to 33 dpa at 573 K and Re atoms in W−2Re irradiated to 33 dpa at 573 K.

the probability of radiation-induced clustering; however no significant clustering was observed in this alloy. After irradiation to 33dpa at 573 K, where only interstitials are significantly mobile [20], any Ta interstitials formed in the W-4.5Ta and W-2Re-1Ta alloy appear to have no detectable tendency to cluster (as evident in the proxigram in Fig. 3c). The hardening in the W-Ta alloys is thus mainly due to radiation-induced dislocation loops, the density of which in W-5Ta saturates at 1.2dpa according to studies by Yi et al. [34]., corresponding to the irradiation hardening plateau above 1.2 dpa observed in W-5Ta by Armstrong et al. [18]. In contrast, when clusters form there is a linear increase in irradiation hardening with dose, as noted by Armstrong et al. for W-5Re under the same

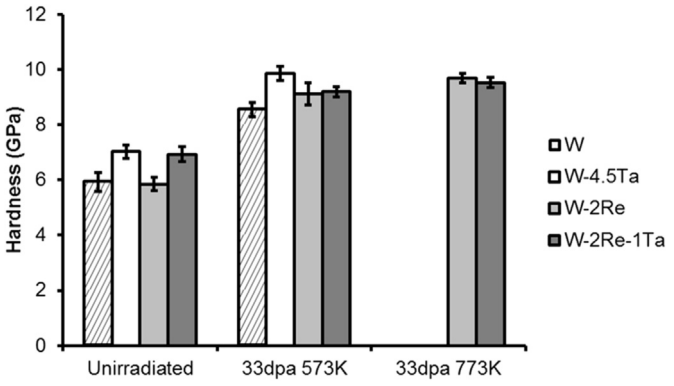

Fig. 7. Nano-hardness of irradiated and unirradiated alloys measured at a depth of 125 nm from the material surface. This depth corresponds to the peak damage level. The hardness data for W irradiated to 33dpa at 573 K are taken from Ref. [19].

Table 3
Hardness values of W, W-4.5Ta, W-2Re and W-2Re-1Ta in the unirradiated condition and after irradiation to 33dpa at 573 K and 773 K. The hardness data of W irradiated to 33dpa at 573 K are taken from Ref. [19].

Alloy	Unirradiated (GPa)	33dpa 573 K (GPa)	33dpa 773 K (GPa)
W	5.93 ± 0.34	8.55 ± 0.25	–
W-4.5Ta	7.02 ± 0.24	9.86 ± 0.26	–
W-2Re	5.85 ± 0.24	9.12 ± 0.4	9.69 ± 0.17
W-2Re-1Ta	6.93 ± 0.28	9.19 ± 0.18	9.52 ± 0.19

irradiation conditions [19].

At 773 K, vacancies are more mobile [20]. For vacancy-mediated diffusion of Ta in tungsten, the activation energy is 6.20 eV and the diffusion constant is 6.20×10^{-4} m^2s^{-1};for Re the values are 6.18 eV and 4.00×10^{-4} m^2s^{-1} [35]. The diffusion coefficient for Ta in W at 773 K is predicted to be 2.3×10^{-44} m^2s^{-1} and for Re in W 2.0×10^{-44} m^2s^{-1}. Though the two solutes have similar diffusion coefficients, Re forms clusters under irradiation and Ta does not. In fact, Ta is depleted within the Re clusters; approaching 0 at.% at the core (Fig. 3c) and having a mean concentration in clusters of 0.17 at.% Ta (Table 2). This lack of formation of tantalum clusters in the binary alloy and the ejection of tantalum from rhenium clusters in the ternary alloys is consistent with the equilibrium binary phase diagrams for W-Ta, Re-Ta and W-Re [36]. Whilst tantalum shows solubility in tungsten across the whole composition range, rhenium shows only limited solubility in tungsten (12 at% at 1500 °C, ≈4 at% at 773 K) and tantalum shows even lower solubility in rhenium (3 at% at 2000 K, ≈2% at 773 K).

While Ta clustering is not observed the presence of Ta affects the clustering behaviour of Re atoms in the W-2Re-1Ta alloy. At 573 and 773 K, the measured cluster number density and volume fraction in W-2Re-1Ta sample is consistently half that in the W-2Re sample. However, Ta has minimal effect on cluster size. The cluster size distribution plots in Fig. 4a–b) for W-2Re-1Ta at 773 K feature the same range (0.5–7 nm) and peak position (3.5 nm) as that of the W-2Re alloy at 773 K. Ta also has negligible effect on Re cluster composition. Fig. 3a–b) and Table 2 shows that the measured Re concentrations in clusters in binary and ternary alloys at each temperature have similar values and fall within the same error bars. Based on these trends, it appears likely that the presence of Ta reduces the nucleation rate of clusters under irradiation. Once a Re cluster forms, Ta has minimal effect on its growth and the level of its Re enrichment.

Comparison to the W-Os-Re alloys studied by Xu et al. [16] show that osmium and tantalum solutes in tungsten behave very differently to each other under identical irradiation conditions, with osmium strongly forming clusters. This is not unexpected, while tantalum is bcc and shows full solubility in tungsten osmium has the hcp structure and shows only limited solubility in tungsten.

Comparisons to neutron-irradiated tungsten are difficult to make due to the large number of experimental variables. Hasegawa and co-workers [37] have conducted TEM studies on a range of irradiated tungsten and tungsten-rhenium alloys. Due to the differing neutron spectra produced in the three different reactors (JOYO, JMTR and HFIR) used for their irradiations, very differing transmutation rates as a function of dpa are produced, all much greater than that expected in a fusion neutron spectrum. At one extreme (HIFR irradiated materials) rhenium precipitates were found at a damage level of 0.9dpa at 500 °C, however the transmutation rate is such that there is 9% Re and 5% Os present at the end of irradiation. In comparison they see no formation of precipitates in an initially pure tungsten sample irradiated in JOYO to 1.54dpa and 750 °C, where the final Re content post-irradiation was only 0.9%. Hasegawa and co-workers have only performed TEM based analysis, with little chemical analysis, which precludes the imaging of the smallest clusters. Our study has the advantage that, using APT, clusters as small as 1 nm can be identified.

4.2. Effect of Ta on irradiation hardening

Comparing solute hardening in the unirradiated alloys, the presence of Ta in the W-2Re-1Ta alloy leads to a stronger overall solid solution hardening effect than in the binary W-2Re alloy, similar to literature hardness data [2]. However, after irradiation, the measured increase in hardness for the W-Re-Ta alloy is 1–1.5 GPa less than in the W-Re alloy at both irradiation temperatures. This is likely to be linked to the W-Re-Ta alloy having a smaller cluster volume fraction than in the W-Re alloy at both irradiation temperatures. This is in contrast to the effect of osmium [16], where a W-1Re-1Os alloy showed higher hardening after ion irradiation (5.38 GPa hardness increase) to 33 dpa at 773 K, compared to that in a W-2Re alloy (3.84 GPa hardness increase) [16,17], associated with a higher cluster density in the W-Re-Os alloy than in the W-Re binary.

Friedel's treatment [38] gives the change in shear yield stress ($\Delta\tau_y$) due to a dispersion of weak (coherent) local obstacles to dislocation motion:

$$\Delta\tau_y = \frac{Gb}{\lambda}[\cos(\phi_c)]^{\frac{3}{2}} \quad [1]$$

where G is the matrix shear modulus (161 GPa), b is the length of the matrix Burgers vector (0.223 nm), ϕ_c is the semi-angle between two arms of dislocations at an obstacle at the point of breakaway. We take $\Delta\tau_y$ as (irradiation hardening)/6 (hardening divided by 3 to give the change in tensile yield stress and then divided by 2 for the change in shear yield stress). The inter-obstacle spacing, λ, is determined as:

$$\lambda = [\rho.d]^{-\frac{1}{2}} - d \quad [2]$$

where ρ is the volume density of obstacles, of diameter d.

Two approaches are possible to what is inevitably a rather approximate estimation of the strength of the clusters as obstacles to dislocation motion, as characterised by ϕ_c. The first is to assume that the hardening from radiation-induced dislocation loops and that from the clusters act independently and additively; this effectively implies that the dislocation loops impede the motion of glide dislocations via long-range stresses, and the clusters by acting as local obstacles. Armstrong et al. [19] found that hardening due to

Table 4
Estimation of ϕ_c, the critical angle dislocations subtend in passing through the clusters, assuming that dislocation loops contribute ~1 GPa of hardening.

Alloy	ΔH at 125 nm (GPa)	ΔH at 125 nm due to clusters (GPa)	$\Delta\tau_y$ [ΔH/6] (GPa)	λ (nm)	ϕ_c (°)
W2Re1Ta 773 K	2.6	1.6	0.26	47	78
W2Re1Ta 573 K	2.3	1.3	0.21	43	83
W2Re 773 K	3.8	2.8	0.47	37	70
W2Re 573 K	3.3	2.3	0.38	30	80

dislocation loop damage in ultra high purity (UHP) tungsten and in a W-5Re alloy saturated at ~13 dpa and gave a hardness increase in both materials of ~1.0 GPa (at higher doses, substantial additional hardening was found in the W-5Re alloy, assumed to be due to Re cluster formation); hence we subtract 1 GPa from the total hardening to give the estimations shown in Table 4 of the critical cluster breakaway angle. The estimations use equation (1), with cluster densities and sizes from Table 2 to derive values of λ via equation (2). Calculated ϕ_c values lie between 70° and 83°. The clusters are weak obstacles to dislocation motion, producing substantial hardening due to their high densities.

A second approach is to assume that the clusters and dislocation loops are separate sets of entities, both acting as local obstacles. A study by Yi et al. [34] gives data for dislocation loop size distributions and densities in UHP tungsten, W5Re and W5Ta self-ion irradiated at 573 K and 773 K. Most of the data are at doses in the range up to 3.6 dpa, with data for 30 dpa irradiation only in pure W at 573 K; in that case, the loop density was ~8.5×10^{22} m^{-3}, with a distribution of loop diameters from ~1 nm (the limit of resolution of the transmission electron microscope used) to >10 nm, and a mean diameter of ~3 nm. Using these data with equations (1) and (2) gives a ϕ_c value of ~85°; so these dislocation loops are also weak obstacles. Yi et al. [34] found that loop densities in the W5Re and W5Ta alloys were roughly twice those in the pure W under the same irradiation conditions; so for the more dilute alloys considered here, a loop density of ~10^{23} m^{-3} might be appropriate. The total obstacle density (loops plus clusters), a weighted average obstacle size and total hardening can then be used to estimate, very roughly, an associated ϕ_c value. Values found were in the range 67°–78°. This also indicates that the clusters are weak obstacles, but the crudity of the method and the difference between the "combined obstacle" ϕ_c and that derived for dislocation loops alone demonstrate that to take analysis of the contributions to hardening of the clusters and loops further, a more sophisticated model would be required, based on more complete information about the distributions of the two obstacle types (including the degree to which loops and clusters are associated with each other).

5. Summary

The influence of Ta on effects of high-dose ion irradiation (33dpa) in W-Ta and W–Re-Ta alloys at 573 K and 773 K was investigated using atom probe tomography and nanoindentation. It was found that:

- Ta in W-Ta and W-2Re-1Ta alloys shows no detectable clustering behaviour after irradiation at temperatures either above and below the vacancy migration onset temperature of ~743 K [20]. Only clustering of Re occurs in the W-2Re-1Ta alloy.
- The cluster number density and volume fraction is reduced where Ta is present in the W-2Re-1Ta alloy. Ta has minimal effect on cluster composition and radius.
- Atom-probe data suggests that Re clusters formed in the W-2Re-1Ta alloy are coherent with the BCC tungsten matrix.
- The irradiation-induced clusters are weak obstacles that individually offer small resistance to dislocation motion. Their hardening effect is based on their high number density. This has also been found for clusters in irradiated W-Re-Os alloys [15].
- As in the case of the W-Re-Os ternary [15], a strong synergistic effect is found between the solutes in the W-Re-Ta alloy. Thus the behaviour under irradiation of ternary or higher order W systems cannot be predicted adequately from studies of binary alloys alone. This is of major significance for the future development of W-based fusion energy materials.

Acknowledgements

This study was supported financially by the EPSRC under Programme grant EP/H018921/1. We thank the Ion Beam Centre (IBC) at the University of Surrey (a National Facility supported by the EPSRC) for performing implantations and Mr C. Salter (University of Oxford) for assistance with EPMA analysis. DEJA acknowledges the funding provided by a Royal Academy of Engineering Research Fellowship. Data is available online on Oxford Research Archive [39].

References

[1] J.W. Davis, V.R. Barabash, A. Makhankov, L. Plochl, K.T. Slattery, Assessment of tungsten for use in the ITER plasma facing components, J. Nucl. Mater. 258–263 (1998) 308–312.
[2] M. Rieth, S.L. Dudarev, S.M.G. de Vicente, J. Aktaa, T. Ahlgren, S. Autusch, D.E.J. Armstrong, M. Balden, N. Baluc, M.F. Barthe, W.W. Basuki, M. Battabyal, C.S. Becquart, D. Blagoeva, H. Boldyryeva, J. Brinkmann, M. Celino, L. Ciupinski, J.B. Correia, A. De Backer, C. Domain, E. Gaganidze, C. Garcia-Rosales, J. Gibson, M.R. Gilbert, S. Giusepponi, B. Gludovatzj, H. Greuner, K. Heinola, T. Hoschen, A. Hoffmann, N. Holstein, F. Koch, W. Krauss, H. Li, S. Lindig, J. Linke, C. Linsmeier, P. Lopez-Ruiz, H. Maier, J. Matejicek, T.P. Mishra, M. Muhammed, A. Munoz, M. Muzyk, K. Nordlund, D. Nguyen-Manh, J. Opschoor, N. Ordas, T. Palacios, G. Pintsuk, R. Pippan, J. Reiser, J. Riesch, S.G. Roberts, L. Romaner, M. Rosinski, M. Sanchez, W. Schulmeyer, H. Traxler, A. Urena, J.G. van der Laan, L. Veleva, S. Wahlberg, M. Walter, T. Weber, T. Weitkamp, S. Wurster, M.A. Yar, J.H. You, A. Zivelonghi, Recent progress in research on tungsten materials for nuclear fusion applications in Europe, J. Nucl. Mater. 432 (2013) 482–500.
[3] S.W.H. Yih, C.T. Wang, Tungsten: Sources, Metallurgy, Properties and Applications, Planum Press, New York, 1979.
[4] V. Tiron, S. Dobrea, C. Costin, G. Popa, On the carbon and tungsten sputtering rate in a magnetron discharge, Nucl. Instrum. Methods Phys. Res. B 267 (2009) 434–437.
[5] M.R. Gilbert, J.-C. Sublet, neutron-induced transmutation effects in W and W-alloys in a fusion environment, Nucl. Fusion 51 (2011) 13.
[6] M.R. Gilbert, S.L. Dudarev, S. Zheng, L.W. Packer, J.-C. Sublet, An integrated model for materials in a fusion power plant: transmutation, gas production, and helium embrittlement under neutron irradiation, Nucl. Fusion 52 (2012) 12.
[7] T. Tanno, A. Hasegawa, M. Fujiwara, J. He, S. Nogami, M. Satou, T. Shishido, K. Abe, Precipitation of solid transmutation elements in irradiated tungsten alloys, Mater. Trans. 49 (2008) 2259–2264.
[8] A. Hasegawa, T. Tanno, S. Nogami, M. Satou, Property change mechanism in tungsten under neutron irradiation, J. Nucl. Mater. 417 (2011) 491–494.
[9] A. Hasegawa, M. Fukuda, S. Nogami, K. Yabuuchi, Neutron irradiation effects on tungsten materials, Fusion Eng. Des. 89 (2014) 1568–1572.
[10] R. Herschitz, D.N. Seidman, An atomic resolution study of homogeneous radiation-induced precipitation in a neutron irradiated W-10at.%Re alloy, Acta Metall. 32 (1984) 1141–1154.
[11] R. Herschitz, D.N. Seidman, An atomic resolution study of radiation-induced precipitation and solute segregation effects in a neutron-irradiated W-25at.%Re alloy, Acta Metall. 32 (1984) 1155–1171.
[12] J. He, G.Y. Tang, A. Hasegawa, K. Abe, Microstructural development and

irradiation hardening of W and W-(3-26) wt% Re alloys after high temperature neutron irradiation to 0.15 dpa, Nucl. Fusion 46 (2006) 877–883.
[13] T. Tanno, A. Hasegawa, J. He, M. Fujiwara, S. Nogami, M. Satou, T. Shishido, K. Abe, Effects of transmutation elements on neutron irradiation hardening of tungsten, Mater. Trans. 48 (2007) 2399–2402.
[14] T. Tanno, M. Fukuda, S. Nogami, A. Hasegawa, Microstructural development in neutron irradiated tungsten alloys, Mater. Trans. 52 (2011) 1447–1451.
[15] D.E.J. Armstrong, X. Yi, E.A. Marquis, S.G. Roberts, Hardening of self ion implanted tungsten and tungsten 5-wt% rhenium, J. Nucl. Mater. 432 (2013) 428–436.
[16] A. Xu, C. Beck, D.E.J. Armstrong, K. Rajan, G.D.W. Smith, P.A.J. Bagot, S.G. Roberts, Ion-irradiation-induced clustering in W-Re and W-Re-Os alloys: a comparative study using atom probe tomography and nanoindentation measurements, Acta Mater. 87 (2015) 121–127.
[17] A. Xu, C. Beck, D.E.J. Armstrong, K. Rajan, G.D.W. Smith, P.A.J. Bagot, S.G. Roberts, Ion-irradiation induced clustering in W-Re and W-Re-Os alloys: a comparative study using atom probe tomography and nanoindentation measurements, Acta Mater. 87 (2015) 121–127.
[18] D.E.J. Armstrong, A.J. Wilkinson, S.G. Roberts, Mechanical properties of ion-implanted tungsten-5 wt% tantalum, Phys. Scr. 2011 (Issue T145) (2011), 014076 (014074pp).
[19] D.E.J. Armstrong, X. Yi, E.A. Marquis, S.G. Roberts, Hardening of self ion implanted tungsten and tungsten 5-wt% rhenium, J. Nucl. Mater. 432 (2013) 428–436.
[20] D.N. Seidman, On the point-defect annealing mechanism for stage III recovery in irradiated or quenched tungsten, Scr. Metall. 13 (1979) 251–257.
[21] J.F. Ziegler, M.D. Ziegler, J.P. Biersack, SRIM - the stopping and range of ions in matter, Nucl. Instrum. Methods Phys. Res. B 268 (2010) (2010) 1818–1823.
[22] D.E.J. Armstrong, T.B. Britton, Effect of dislocation density on improved radiation hardening resistance of nano-structured tungsten-rhenium, Mater. Sci. Eng. A 611 (2014) 388–393.
[23] T.F. Kelly, M.K. Miller, Invited review article: atom probe tomography, Rev. Sci. Instrum. 78 (2007) 031101.
[24] K. Thompson, D. Lawrence, D.J. Larson, J.D. Olson, T.F. Kelly, B. Gorman, In situ site-specific specimen preparation for atom probe tomography, Ultramicroscopy 107 (2007) 131–139.
[25] B. Gault, M.P. Moody, F. Geuser, G. Tsafnat, A. Fontaine, L.T. Stephenson, D. Haley, S.P. Ringer, Advances in the calibration of atom probe tomographic reconstruction, J. Appl. Phys. 105 (2009) 034913.
[26] J.M. Hyde, C.A. English, An analysis of the structure of irradiation induced Cu-enriched clusters in low and high nickel welds, Microstruct. Process. Irradiat. Mater. 650 (2001) R6.6.1–R6.6.12. Boston.
[27] J.M. Hyde, E.A. Marquis, K.B. Wilford, T.J. Williams, A sensitivity analysis of the maximum separation method for the characterization of solute clusters, Ultramicroscopy 111 (2011) 440–447.
[28] M.C. Oliver, G.M. Pharr, Improving technique for determining hardness and elastic modulus using load and displacement sensing indentation experiments, J. Mater. Res. 7 (1992) 1564–1580.
[29] C. Berne, M. Sluiter, Y. Kawazoe, T. Hansen, A. Pasturel, Site occupancy in the Re-W sigma phase, Phys. Rev. B 64 (2001).
[30] G.A. Cottrell, Sigma phase formation in irradiated tungsten, tantalum and molybdenum in a fusion power plant, J. Nucl. Mater. 334 (2004) 166–168.
[31] C.D. Elvin, Identification of rhenium in tungsten-rhenium alloys using field-ion microscope, Philos. Mag. 16 (1967), 35-&.
[32] A.L. Field, R.L. Ammon, A.L. Lewis, L.S. Richardson, Research and development of tantalum and tungsten based alloys, in: Navy BoNW (Ed.), Westinghouse Research Laboratories, Pittsburgh 35, Pennsylvania, 1961, p. 199.
[33] S. Wurster, B. Gludovatz, A. Hoffmann, R. Pippan, Fracture behaviour of tungsten-vanadium and tungsten-tantalum alloys and composites, J. Nucl. Mater. 413 (2011) 166–176.
[34] X. Yi, M.L. Jenkins, K. Hattar, P.D. Edmondson, S.G. Roberts, Characterisation of radiation damage in W and W-based alloys from 2 MeV self-ion near-bulk implantations, Acta Mater. 90 (2015) 163–177.
[35] G. Neumann, C. Tuijn, Self-diffusion and Impurity Diffusion in Pure Metals, Elsevier, United Kingdom, 2009.
[36] T.B. Massalski, H. Okamoto, P.R. Subramanian, L. Kacprzak, Binary Alloy Phase Diagrams, 2 ed., ASM International, 1990.
[37] A. Hasegawa, M. Fukuda, K. Yabuuchi, S. Nogami, Neutron irradiation effects on the microstructural development of tungsten and tungsten alloys, J. Nucl. Mater. 471 (2016) 175–183.
[38] M.W. Lui, I. Le May, On the "friedel relation" in precipitation hardening, Scr. Metall. 9 (1975) 587–589.
[39] Ion-irradiation induced clustering in W-Re-Ta, W-Re and W-Ta alloys: An atom probe tomography and nanoindentation study data. http://dx.doi.org/10.5287/bodleian:Vje1pQOa5.